The 2D AKLT state is a universal quantum computational resource

Tzu-Chieh Wei, Ian Affleck, and Robert Raussendorf
Department of Physics and Astronomy, University of British Columbia, Vancouver, British Columbia V6T 1Z1, Canada
(Dated: September 16, 2010)

We demonstrate that the two-dimensional AKLT state on a honeycomb lattice is a universal resource for measurement-based quantum computation. Our argument proceeds by reduction of the AKLT state to a 2D cluster state, which is already known to be universal, and consists of two steps. First, we devise a local POVM by which the AKLT state is mapped to a random 2D graph state. Second, we show by Monte Carlo simulations that the connectivity properties of these random graphs are governed by percolation, and that typical graphs are in the connected phase. The corresponding graph states can then be transformed to 2D cluster states.

PACS numbers:

I. INTRODUCTION

Quantum computation promises exponential speedup over classical computation by exploiting the quantum mechanical nature of physical processes, such as unitary evolution, superposition and measurement [1]. In addition to the standard circuit models and adiabatic evolution of quantum computation based on unitarity, surprisingly, local measurement alone provides the same power of computation, given only a prior sufficiently entangled state [2]. Cluster states are the first known resource states for such measurement-based quantum computation (MBQC) [2, 3]. Cluster states of small size were created with photons [4]. They can also be created with active Ising-type interactions, and were demonstrated in cold-atom systems [5]. They also arise as the unique ground state of *five-body* interacting Hamiltonian on a square lattice; however, they cannot be the exact unique ground state of any *two-body* Hamiltonian [6, 7]. Fundamentally, could there be unique ground states of any two-body interacting Hamiltonian that are universal resources?

Indeed, resource states other than cluster states for MBQC were later devised via a valence-bond-solid picture, and the computation is performed in the so-called correlation space [8, 9]. These states can have local Hilbert-space dimension greater than that of a spin-1/2. For example, the 1D spin-1 AKLT state [10], first appearing in connection with Haldane's conjecture on the spectral gap of isotropic integer-spin chains [11], can actually be used to implement one-qubit gates [9, 12]. This was recently demonstrated with photons [13]. Even though 1D AKLT chains alone are not sufficient for universal quantum computation, further active coupling of many such chains can in principle implement quantum computation [14].

A universal resource state can therefore only exist in spatial dimensions greater than one. In searching for such resourceful ground states of physically reasonable Hamiltonians, Chen et al. made some important progress by constructing a spin-5/2 resourceful state on a honeycomb lattice, which is an unique ground state of a two-body interacting Hamiltonian [15]. Later Cai et al. approached this issue by patching ground states of AKLT chains (of mixed spin-3/2 and spin-1/2 entities) into an effective 2D spin-3/2 state [16]. This construction reduced the local Hilbert-space dimension from 6 of Chen et al. [15] to 4. However, both engineered Hamiltonians, even though consisting of only two-body interaction, turn out be complicated and possess less symmetry than the original AKLT Hamiltonians.

It remains open whether any of the original 2D AKLT states can be universal resources for MBQC. Here we show that this is indeed the case. The ground state of the AKLT model (of spin-3/2) on the 2D honeycomb lattice can be reduced to a two-dimensional cluster state by local operations. This transformation proceeds in two steps. First, the AKLT state is mapped to a random encoded graph state by a local POVM. Second, if this graph state is sufficiently connected, it can be further transformed by local measurements into a two-dimensional cluster state. In a Monte Carlo simulation, we demonstrate that the required connectivity properties hold for typical graphs. Beyond honeycomb, our method applies to any trivalent lattice.

II. AKLT STATES, GRAPH STATES AND THE REDUCTION

In order to show that a state can be universal for MBQC, there are two possible routes: (1) by constructing an measurement scheme for universal gates, as was done in the original one-way computer [2] or the valence-bond approach [8, 9]; (2) by showing that the state can be converted to any of the existing known resource states [17–19] by local measurement, such as the cluster state [3]. We shall adopt the latter route and show that the AKLT state can be reduced to a cluster state.

The AKLT state on the two-dimensional honeycomb $\mathcal{L}$ can be described in the following way. First, each vertex or site v of $\mathcal{L}$ contains three virtual spin-1/2 particles, lying at the ends of the three incoming edges (or bonds). The two virtual spins residing on the two ends of an edge $e = \{u, v\}$ linking the two nearest neighbors u and v are in the singlet state: $|\phi\rangle_e \equiv |01\rangle - |10\rangle$ (omitting the

normalization). (Note that $|0\rangle \equiv |\uparrow\rangle$ and $|1\rangle \equiv |\downarrow\rangle$ are the two basis states of spin-1/2.) Then at each lattice site v, a projection is made on the three virtual spins into the symmetric subspace

$$P_{S,v} \equiv |000\rangle\langle 000| + |W\rangle\langle W| + |\overline{W}\rangle\langle\overline{W}| + |111\rangle\langle 111|, \quad (1)$$

$$|W\rangle \equiv \frac{1}{\sqrt{3}}(|001\rangle + |010\rangle + |100\rangle), \quad (2)$$

$$|\overline{W}\rangle \equiv \frac{1}{\sqrt{3}}(|110\rangle + |101\rangle + |011\rangle), \quad (3)$$

where the four states $|000\rangle$, $|111\rangle$, $|W\rangle$ and $|\overline{W}\rangle$ constitute the basis states for the symmetric subspace of three spin-1/2 particles and they can also be regarded as the four basis states for a spin-3/2 particle $|3/2, 3/2\rangle$, $|3/2, -3/2\rangle$, $|3/2, 1/2\rangle$ and $|3/2, -1/2\rangle$, respectively, via the standard addition of angular momenta. Thus the AKLT state on the honeycomb lattice can be viewed as one with three virtual spin-1/2 particles per site, written as

$$|\text{AKLT}\rangle := \bigotimes_{v\in V(\mathcal{L})} P_{S,v} \bigotimes_{e\in E(\mathcal{L})} |\phi\rangle_e, \quad (4)$$

where we use $V(\mathcal{L})$ and $E(\mathcal{L})$ to denote the set of vertices and edges, respectively, of graph $\mathcal{L}$. This virtual spin-1/2 picture can also be described by a Schwinger boson representation [20], and is particularly useful in constructing a graph state via the stabilizer formalism, discussed below. The AKLT state can also be regarded a state of spin-3/2 particles via a further mapping at each site $Q \equiv |3/2, 3/2\rangle\langle 000| + |3/2, -3/2\rangle\langle 111| + |3/2, 1/2\rangle\langle W| + |3/2, -1/2\rangle\langle\overline{W}|$). The resultant spin-3/2 AKLT state is the unique ground state of a spin-3/2 isotropic two-body Hamiltonian and has exponential decay in the correlations, indicating a gap in the spectrum [10].

Next, we give the definition of a graph state $|G\rangle$ of graph G, to which we shall prove that the AKLT state can be locally converted. A graph state is defined via the invariance under the action of a set of commuting operators K_v (namely, the stabilizer generators) [3, 21]

$$K_v|G\rangle = |G\rangle, \ \forall v \in V(G), \quad (5)$$

$$K_v \equiv X_v \bigotimes_{u\in \text{nb}(v)} Z_u = X_v \bigotimes_{u\in V(G)} (Z_u)^{[A(G)]_{uv}}, \quad (6)$$

where $\text{nb}(v)$ denotes the neighbors of vertex v, i.e., the subset of vertices that are connected to v via an edge in the graph G, $A(G)$ is the adjacency matrix of the graph G [22] and $X \equiv \sigma_x$, $Y \equiv \sigma_y$ and $Z \equiv \sigma_z$ are the three Pauli matrices. A cluster state is an example of graph states with the underlying graph being a regular lattice, such as the square lattice. Any 2D cluster state is a universal resource for measurement-based quantum computation [2, 17].

The main result of our paper is to show that the 2D AKLT state can be locally converted to a 2D cluster state, therefore establishing the AKLT state as a universal resource. We outline key steps to establish this universality.

(1) We employ a positive-operator-value-measure (POVM) or generalized measurement for all sites that takes locally the three virtual spin-1/2 states (or equivalently a spin-1 state) to an effective spin-1/2 state. To be specific, on every site $v \in V(\mathcal{L})$ the POVM consists of three rank-two elements [23]

$$\begin{aligned} F_{v,z} &= \sqrt{\frac{2}{3}}\frac{I_{12}+Z_1Z_2}{2}\frac{I_{23}+Z_2Z_3}{2}, \\ F_{v,x} &= \sqrt{\frac{2}{3}}\frac{I_{12}+X_1X_2}{2}\frac{I_{23}+X_2X_3}{2}, \\ F_{v,y} &= \sqrt{\frac{2}{3}}\frac{I_{12}+Y_1Y_2}{2}\frac{I_{23}+Y_2Y_3}{2}. \end{aligned} \quad (7)$$

Therein, $\{1, 2, 3\} = v$ are the qubit locations at a given vertex $v \in V(\mathcal{L})$. Physically, $F_{v,a}$ is actually proportional to a projection operator onto $S_a = \pm 3/2$ states. The above POVM elements obey the relation $\sum_{\nu\in\{x,y,z\}} F^\dagger_{v,\nu}F_{v,\nu} = I_{v,\text{sym}}$, i.e., project onto the symmetric subspace, as required. The outcome of POVM is random and can be either x, y or z.

(2) The random outcome of the POVM gives rise to a random graph and hence a random graph state, labeled by $|G(\mathcal{A})\rangle$. We establish the properties of a *typical* random graph: (a) The size distribution of the clusters (defined below) is microscopic, i.e., independent of the lattice size, and (b) the existence of a path traversing the graph from, e.g., the left-most side to the right-most side, with close to unity probability. These properties ensure the typical graph state is universal for measurement based quantum computation. (3) Finally, we numerically demonstrate these properties by Monte Carlo simulations.

III. REDUCTION OF THE 2D HONEYCOMB AKLT STATE TO A GRAPH STATE

To show that the 2D AKLT state is a resource for quantum computation by local operations, we first show that it can be mapped to a graph state by local POVMs. The resulting graph state depends on the random (but short-range correlated) POVM outcomes. We are interested in the connectivity properties of resulting typical graphs.

After the POVM has been performed on every site, the resulting state becomes (depending on the outcome $a_v \in \{x, y, z\}$ on vertex v)

$$|\Psi(\mathcal{A})\rangle := \bigotimes_{v\in V(\mathcal{L})} F_{v,a_v}\,|\text{AKLT}\rangle \sim \bigotimes_{v\in V(\mathcal{L})} F_{v,a_v} \bigotimes_{e\in E(\mathcal{L})} |\phi\rangle_e, \quad (8)$$

where $\mathcal{A} = \{a_v, v \in V(\mathcal{L})\}$ is the set of outcomes of the local POVMs.

Reduction to a graph state. It turns out that, for any $\mathcal{A}$, the state $|\Psi(\mathcal{A})\rangle$ is local equivalent to an encoded graph state $\overline{|G(\mathcal{A})\rangle}$, with the graph $G(\mathcal{A})$ constructed as follows. An edge $(v, w) \in E(\mathcal{L})$ is called internal iff

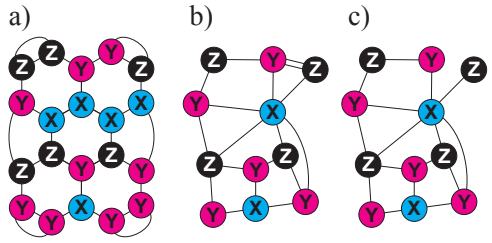

FIG. 1: Graphical rules for transformation of an AKLT state into an encoded graph state by the local POVMs Eq. (7). a) AKLT state on a honeycomb lattice $\mathcal{L}$, with a random pattern $\mathcal{A}$ of local POVM outcomes x, y, z. b) Edges of $\mathcal{L}$ with same-type endpoints are contracted. c) Edges of even multiplicity are deleted, edges of odd multiplicity are converted into standard edges. The resulting graph is $G(\mathcal{A})$. The vertex labels now specify the encoding (9) of the graph state $|G(\mathcal{A})\rangle$.

at the sites v and w the local POVM has resulted in the same outcome. The graph $G(\mathcal{A})$ is obtained from the lattice graph $\mathcal{L}$ by (1) contracting all internal edges, and, in the resultant multi-graph, (2a) deleting all edges of even multiplicity and (2b) converting all edges of odd multiplicity into conventional edges of multiplicity 1. See Fig. 1 for illustration.

In step (1) of the above procedure, several sites of $\mathcal{L}$ are merged into a single composite object $\mathcal{C} \in V(G(\mathcal{A}))$. Each such $\mathcal{C}$ is both a *vertex* in the graph $G(\mathcal{A})$ and a connected set of same-type sites of $\mathcal{L}$, i.e., a *domain*. Physically, in a domain of type a, we have anti-ferromagnetic order along the $\pm a$-direction, because two neighboring spins never have the same $S_a = 3/2$ (or -3/2) in the AKLT state [10].

The outlined construction leads to

Theorem 1 *For any $\mathcal{A}$ that specifies all outcomes of POVMs on $\mathcal{L}$, quantum computation by local spin-3/2 measurements on the state $|\Psi(\mathcal{A})\rangle$ can efficiently simulate quantum computation by local spin-1/2 measurement on the graph state $|G(\mathcal{A})\rangle$.*

Thus, the computational power of the AKLT state, as harnessed by the POVMs Eq. (7), hinges on the connectivity properties of $G(\mathcal{A})$. If, for typical sets $\mathcal{A}$ of POVM outcomes, the graph state $|G(\mathcal{A})\rangle$ is computationally universal then so is the AKLT state. Below we prove Theorem 1, and subsequently display our numerical findings on the connectedness of $G(\mathcal{A})$.

Proof of Theorem 1. The proof proceeds in three steps. First we show that every domain $\mathcal{C} \in V(G(\mathcal{A}))$ gives rise to one encoded qubit. Second, we show that $|\Psi(\mathcal{A})\rangle$ is, up to local encoded unitaries, equivalent to the encoded graph state $\overline{|G(\mathcal{A})\rangle}$. Third, we show that the encoding can be unraveled by local spin-3/2 measurements.

Step 1: Encoding. Consider a domain $\mathcal{C} \subset V(\mathcal{L})$. That is, on all sites $v \in \mathcal{C}$ the same POVM outcome $a \in \{x, y, z\}$ was obtained. $\mathcal{C}$ contains $3|\mathcal{C}|$ qubits. The projections $F_{v,a}$ on all $v \in \mathcal{C}$ enforce $2|\mathcal{C}|$ stabilizer generators, c.f. Eq. (7). Furthermore, choose a tree $\mathcal{T}$ among the set of edges with both endpoints in the domain $\mathcal{C}$. Each edge $(u, v) \in \mathcal{T}$ contributes a stabilizer generator $-\sigma_a^{(u)}\sigma_a^{(v)}$ to the product of Bell states $\bigotimes_{e\in E(\mathcal{L})} |\phi\rangle_e$. These stabilizers commute with the local POVMs (7) and therefore are also stabilizer generators for $|\Psi(\mathcal{A})\rangle$, c.f. Eq. (8). Since $|\mathcal{T}| = |\mathcal{C}| - 1$, in total there are $3|\mathcal{C}| - 1$ stabilizer generators with support only in $\mathcal{C}$, acting on $3|\mathcal{C}|$ qubits. They give rise to one encoded qubit.

While the stabilizer generators for our code follow from the construction, there is freedom in choosing the encoded Pauli operators. We make the following choice:

POVM outcome	z	x	y
stabilizer generator	$\lambda_i\lambda_{i+1}Z_iZ_{i+1}$,	$\lambda_i\lambda_{i+1}X_iX_{i+1}$	$\lambda_i\lambda_{i+1}Y_iY_{i+1}$
$\overline{X}$	$\bigotimes_{j=1}^{3\|\mathcal{C}\|} X_j$	$\bigotimes_{j=1}^{3\|\mathcal{C}\|} Z_j$	$\bigotimes_{j=1}^{3\|\mathcal{C}\|} Z_j$
$\overline{Z}$	$\lambda_i Z_i$	$\lambda_i X_i$	$\lambda_i Y_i$

(9)

In the first line of Eq. (9), $i = 1\,..\,3|\mathcal{C}| - 1$, and in the third line $i = 1\,..\,3|\mathcal{C}|$. $\mathcal{L}$ is bicolorable, $V(\mathcal{L}) = B \cup W$. Then, $\lambda_i = 1$ if $i \in v \in W$ and $\lambda_i = -1$ if $i \in v' \in B$.

Step 2: We show that $|\Psi(\mathcal{A})\rangle$ is an encoded graph state. Consider a central vertex $\mathcal{C}_c \in V(G(\mathcal{A}))$ and all its neighboring vertices $\mathcal{C}_\mu \in V(G(\mathcal{A}))$. Denote the POVM outcome for all $\mathcal{L}$-sites $v \in \mathcal{C}_c, \mathcal{C}_\mu$ by a_c and a_μ, respectively. Denote by E_μ the set of $\mathcal{L}$-edges that run between $\mathcal{C}_c$ and $\mathcal{C}_\mu$. Denote by E_c the set of $\mathcal{L}$-edges internal to $\mathcal{C}_c$. Denote by C_c the set of all qubits in $\mathcal{C}_c$, and by C_μ the set of all qubits in $\mathcal{C}_\mu$. (Recall that there are 3 qubit locations per $\mathcal{L}$-vertex $v \in \mathcal{C}_c, \mathcal{C}_\mu$.) We first consider the stabilizer of the state $\bigotimes_{e\in E(\mathcal{L})} |\phi\rangle_e$. For any μ and any edge $e \in E_\mu$, let $u(e)$ $[v(e)]$ be the endpoint of e in C_μ $[C_c]$. Then, for all μ and all $e \in E_\mu$ the Pauli operators $-\sigma_{a_\mu}^{(u(e))}\sigma_{a_\mu}^{(v(e))}$ are in the stabilizer of $\bigotimes_{e\in E(\mathcal{L})} |\phi\rangle_e$. Choose $b \in \{x, y, z\}$ such that $b \neq a_c$, and let, for any edge $e' \in E_c$, $v_1(e'), v_2(e') \in C_c$ be qubit locations such that $e' = (v_1(e'), v_2(e'))$. Then, for all $e' \in E_c$, $-\sigma_b^{(v_1(e'))}\sigma_b^{(v_2(e'))}$ is in the stabilizer of $\bigotimes_{e\in E(\mathcal{L})} |\phi\rangle_e$. Therefore, the product of all these operators,

$$O_{\mathcal{C}_c} = \pm \left(\bigotimes_\mu \bigotimes_{e\in E_\mu} \sigma_{a_\mu}^{(u(e))}\sigma_{a_\mu}^{(v(e))} \right) \left(\bigotimes_{e'\in E_c} \sigma_b^{(v_1(e'))}\sigma_b^{(v_2(e'))} \right) \tag{10}$$

is also in the stabilizer of $\bigotimes_{e\in E(\mathcal{L})} |\phi\rangle_e$.

We now show that $O_{\mathcal{C}_c}$ commutes with the local POVMs and is therefore also in the stabilizer of $|\Psi(\mathcal{A})\rangle$. First, consider the central domain $\mathcal{C}_c$. The operator $O_{\mathcal{C}_c}$ acts non-trivially on every qubit in C_c, $O_{\mathcal{C}_c}|_l \neq I_l$ for all qubits $l \in C_c$. Furthermore, for all qubits $l \in C_c$, $O_{\mathcal{C}_c}|_l \neq \sigma_{a_c}^{(l)}$. Namely, if $l \in C_c$ is connected by an edge $e \in E_\mu$ to $\mathcal{C}_\mu$, for some μ, then $O_{\mathcal{C}_c}|_l = \sigma_{a_\mu}^{(l)} \neq \sigma_{a_c}^{(l)}$ (for all μ, $a_\mu \neq a_c$ by construction of $G(\mathcal{A})$). Or, if $l \in C_c$ is the endpoint of an internal edge $e' \in E_c$ then $O_{\mathcal{C}_c}|_l = \sigma_b^{(l)} \neq \sigma_{a_c}^{(l)}$ ($a_c \neq b$ by above choice). There-

fore, for any $i,j \in C_c$, $O_{\mathcal{C}_c}$ anticommutes with $\sigma_{a_c}^{(i)}$ and $\sigma_{a_c}^{(j)}$, and thus commutes with all $\sigma_{a_c}^{(i)}\sigma_{a_c}^{(j)}$. Thus, $O_{\mathcal{C}_c}$ commutes with the local POVMs Eq. (7) on all $v \in \mathcal{C}_c$.

Second, consider the neighboring domains $\mathcal{C}_\mu$. $O_{\mathcal{C}_c}\big|_{\mathcal{C}_\mu} = \bigotimes_j \sigma_{a_\mu}^{(j)}$ by construction. $O_{\mathcal{C}_0}$ thus commutes with the local POVMs F_{v,a_μ} for all $v \in \mathcal{C}_\mu$ and for all μ.

Therefore, $O_{\mathcal{C}_c}$ is in the stabilizer of $|\Psi(\mathcal{A})\rangle$. Therefore, $O_{\mathcal{C}_c}$ is an encoded operator w.r.t. the code Eq. (9), and we need to figure out which one. (1) Central vertex $\mathcal{C}_c$: $O_{\mathcal{C}_c}|_{C_c}$ is an encoded operator on C_c, $O_{\mathcal{C}_c}|_{C_c} \in \{\pm\overline{I}, \pm\overline{X}, \pm\overline{Y}, \pm\overline{Z}\}$. Since $O_{\mathcal{C}_c}|_l \neq \sigma_{a_c}^{(l)}$ for any $l \in \mathcal{C}_c$, by Eq. (9), $O_{\mathcal{C}_c}|_{C_c} \neq \pm\overline{I}, \pm\overline{Z}$. Thus, $O_{\mathcal{C}_c}|_{C_c} \in \{\pm\overline{X}, \pm\overline{Y}\}$. (2) Neighboring vertices $\mathcal{C}_\mu$: By Eq. (9), $\sigma_{a_\mu}^{(l)} = \pm\overline{Z}$, for any $l \in C_\mu$. Thus, $O_{\mathcal{C}_c}|_{C_\mu} = \pm\overline{Z}^{|E_\mu|}$. Now observe that $Z^2 = I$, and that, this justifies the above prescription in constructing the graph $G(\mathcal{A})$. Using the adjacency matrix $A_{G(\mathcal{A})}$, we have $|E_\mu| \mod 2 = [A_{G(\mathcal{A})}]_{c,\mu}$ and hence $O_{\mathcal{C}_c}|_{C_\mu} = \pm\overline{Z}^{[A_{G(\mathcal{A})}]_{c,\mu}}$.

Thus, finally, for all $\mathcal{C}_c \in V(G(\mathcal{A}))$,

$$O_{\mathcal{C}_c} \in \left\{ \pm\overline{R}_{C_c} \bigotimes_{\mathcal{C}_\mu \in V(G(\mathcal{A}))} \overline{Z}_{\mathcal{C}_\mu}^{[A_{G(\mathcal{A})}]_{c,\mu}}, \text{ with } R = X, Y \right\} \tag{11}$$

This is, up to conjugation by one of the local encoded gates $\overline{I}_{\mathcal{C}_c}, \overline{Z}_{\mathcal{C}_c}, \exp\left(\pm i\pi/4\, \overline{Z}_{\mathcal{C}_c}\right)$ [see Eq. (6)], a stabilizer generator for the encoded graph state $\overline{|G(\mathcal{A})\rangle}$. The code stabilizers Eq. (9) and the stabilizer operators in Eq. (11) together define the state $|\Psi(\mathcal{A})\rangle$ uniquely. $|\Psi(\mathcal{A})\rangle$ is, up to the action of local encoded phase gates, an encoded graph state $|G(\mathcal{A})\rangle$.

Step 3: Decoding of the code Eq. (9). We show that any domain $\mathcal{C} \in V(G(\mathcal{A}))$ can be reduced to a single elementary site $w \in V(\mathcal{L})$ by local measurement on all other sites $v \in \mathcal{C}$, $v \neq w$. For any such v, choose the measurement basis $\mathcal{B}_a$, $a \in \{x, y, z\}$, as follows

$$\begin{aligned} \mathcal{B}_x &= \left\{(|+++\rangle \pm |---\rangle)/\sqrt{2}\right\}, \\ \mathcal{B}_y &= \left\{(|i,i,i\rangle \pm |-i,-i,-i\rangle)/\sqrt{2}\right\}, \\ \mathcal{B}_z &= \left\{(|000\rangle \pm |111\rangle)/\sqrt{2}\right\}. \end{aligned} \tag{12}$$

These measurements map the symmetric subspace of the three-qubit states into itself and they can therefore be performed on the physical spin 3/2 systems.

Denote by $\mathcal{S}_\mathcal{C}$ and $\mathcal{S}_{\mathcal{C}\setminus v}$ the code stabilizer on the domain $\mathcal{C} \in V(G(\mathcal{A}))$ and on the reduced domain $\mathcal{C}\setminus v$, respectively. Using standard stabilizer techniques [21] it can be shown that the measurement Eq. (12) has the following effect on the encoding

$$\mathcal{S}_\mathcal{C} \longrightarrow \mathcal{S}_{\mathcal{C}\setminus v},\ \overline{X}_\mathcal{C} \longrightarrow \pm\overline{X}_{\mathcal{C}\setminus v},\ \overline{Z}_\mathcal{C} \longrightarrow \overline{Z}_{\mathcal{C}\setminus v}. \tag{13}$$

The measurement (12) thus removes from $\mathcal{C}$ by one lattice site $v \in V(\mathcal{L})$. We repeat the procedure until only one site, w, remains in $\mathcal{C}$, for each $\mathcal{C} \in V(G(\mathcal{A}))$. In this way, $\mathcal{S}_\mathcal{C} \longrightarrow \mathcal{S}_{\{w\}}$, $\overline{X}_\mathcal{C} \longrightarrow \pm\overline{X}_{\{w\}}$, $\overline{Z}_\mathcal{C} \longrightarrow \overline{Z}_{\{w\}}$. Thus, $|\Psi(A)\rangle \longrightarrow \overline{U}_{\rm loc}|\overline{G(A)}\rangle =: |G(A)\rangle$, where $U_{\rm loc}$ is a local unitary, and the encoding Eq. (9) has now shrunk to one site of $\mathcal{L}$ per encoded qubit, i.e. to three auxiliary qubits.

To complete the computation, the remaining encoded qubits are measured individually. Again, the measurement of an encoded qubit on a site $w \in \mathcal{L}$ is an operation on the symmetric subspace of three auxiliary qubits at w, and can thus be realized as a measurement on the equivalent physical spin 3/2. □

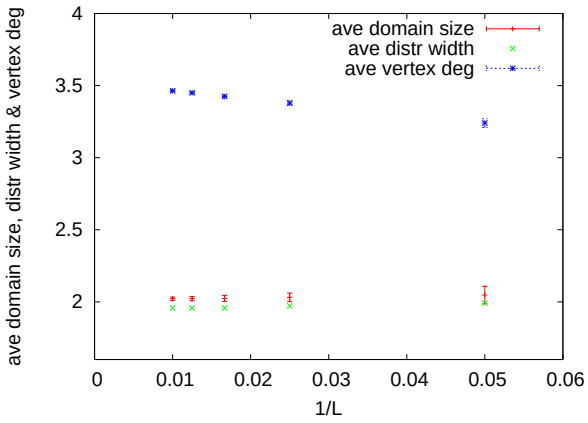

FIG. 2: (color online) Average domain size, average width of domain size distribution, and average degree of a vertex in the typical random graphs vs. L, where L^2 is the total number of sites in the honeycomb lattice. For better discernibility of the two lower sets of data, we suppress the errorbars for one of them.

IV. RANDOM GRAPH $G(\mathcal{A})$ CONTAINS 2D LATTICE GRAPH ABOVE PERCOLATION THRESHOLD

For a large initial lattice $\mathcal{L}$ the random graph state $|G(\mathcal{A})\rangle$ can, with close to unit probability, be efficiently reduced to a large two-dimensional cluster state if the following two properties hold:

1. The size distribution of the domains is *microscopic*, i.e., is independent of the size of the lattice $\mathcal{L}$ in the limit of large $\mathcal{L}$.

2. The probability of existence of a path through $G(\mathcal{A})$ from the left to the right approaches unity in the limit of large $\mathcal{L}$.

Condition 1 is related to the property of the AKLT state having only short range antiferromagnetic order, i.e., no long range Neél order. Hence, it implies that the graph $G(\mathcal{A})$ resulting from the contraction of internal edges of $\mathcal{L}$ only has short-range edges. The connectedness of $G(\mathcal{A})$ is thus a percolation problem. Then, Condition 2 ensures that the system is above the percolation

threshold, i.e., in the connected phase. A macroscopically extended connected component in $G(\mathcal{A})$ is necessary for universal measurement-based quantum computation with $|G(\mathcal{A})\rangle$. If no such component is present, measurement-based QC on $|G(\mathcal{A})\rangle$ is essentially local and can therefore be efficiently classically simulated; see also Ref. [24].

More importantly, being above the percolation threshold is also *sufficient* for the reduction of the random graph state $|G(\mathcal{A})\rangle$ to a standard universal cluster state. This has been shown in [24], where the reduction to a 2D cluster state on a hexagonal lattice was demonstrated. In Appendix A we present an alternative argument for the reduction of a random graph state $|G(\mathcal{A})\rangle$ to a 2D cluster state on a rectangular lattice, above the percolation threshold.

We used Monte Carlo simulations to compute the properties of the typical random graphs resulting from the POVM. The simulations utilize a generalized Hoshen-Kopelman algorithm [25] to identify domains and a Metropolis method to sample typical random graphs; see Appendix B for details. The average degree of vertices in the typical random graphs is about 3.52, when extrapolated to an infinite system size. Furthermore, the typical random graphs retain large number of vertices, edges, and independent cycles, with $|\bar{V}| \approx 0.496L^2$, $|\bar{E}| \approx 0.872L^2$, and the Betti number [26] $\bar{B} \approx 0.377L^2$, respectively, where we take the number of vertices on a honeycomb lattice to be $N \equiv L^2$.

We check by simulations that Condition 1 is satisfied. Maximal domain that contains the largest number of the original sites of identical POVM outcome is indeed never macroscopic. The average number of the original sites contained in a typical domain, when extrapolated to the infinite system, is about 2.02 and the width in the domain size distribution is extrapolated to about 1.95; see Fig. 2. Next, to demonstrate that the typical random graphs are well connected, we study their percolation properties (i.e., the existence of a spanning cluster). We investigate how robust it is upon, e.g., deleting edges probabilistically, i.e., the bond percolation. As shown in Fig. 3, it requires the probability of deleting to be as high $p^*_{\rm delete} \approx 0.43$ (i.e., percolation threshold $p_{\rm th} \equiv 1 - p^*_{\rm delete} \approx 0.57$) in order to destroy the spanning property of the graph. These results demonstrate Conditions 1 and 2 are satisfied and the resultant typical random graph states are therefore universal resources for MBQC.

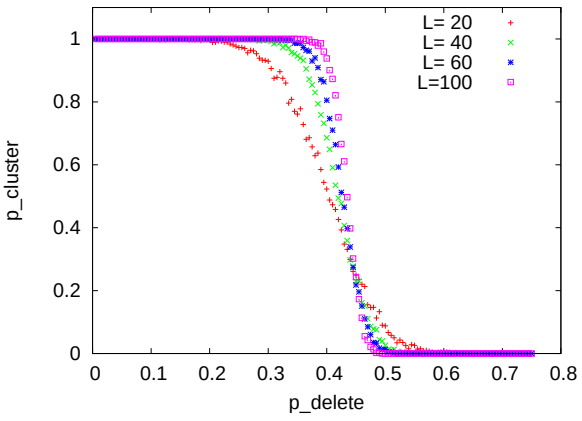

FIG. 3: (color online) Percolation study of the graph formed by the domains: probability of a spanning cluster $p_{\rm cluster}$ vs. the probability to delete an edge $p_{\rm delete}$. The threshold for destroying the spanning cluster is around $p_{\rm delete} = 1 - p_{\rm th} \approx 0.43$. This shows that the graph is deep in the percolated (i.e., connected) phase.

V. CONCLUDING REMARKS

We investigated the issue of whether any of the originally proposed 2D AKLT states can be universal resource states for measurement-based quantum computation. We demonstrated that the two-dimensional spin-3/2 AKLT state on a honeycomb lattice is indeed a universal resource. In particular, we showed the AKLT state can be locally reduced to a random graph state by an appropriately devised POVM at each site. Our Monte Carlo simulations showed that the underlying graphs for such typical graph states possess connectivity properties in the percolated phase, and therefore the resultant typical graph states can be further converted to 2D cluster state locally, which is already known to be a universal resource for quantum computation.

The Hamiltonian for the 2D AKLT is two-body interacting and invariant under spin rotation. The AKLT state is the unique ground state, and Neél states cannot occur in the AKLT Hamiltonian. It is generally believed that there is a spectral Haldane gap, just like the 1D integer-spin chains. In line with a recent study by Miyake [12], we end by raising the following question: assume there is a Haldane-like phase around the 2D AKLT state as is the case in the 1D bilinear-biquardratic model, are all the ground states in such a 2D Haldane phase computationally useful?

Acknowledgment. This work was supported by NSERC, MITACS, and CIFAR.

Appendix A: Reduction of $|G(\mathcal{A})\rangle$ to a 2D cluster state above the percolation threshold

Conditions 1, 2 in Sec. IV are also sufficient for computational universality. To see this, consider a large typical graph $G(\mathcal{A})$ obeying Condition 1, and regions α, β, A, B, .. imposed on it as displayed in Fig. 4 a. The regions α, β, .. are ring-shaped and spread upon $G(\mathcal{A})$ as nodes of a two-dimensional grid. The regions A, B, .. are of rect-

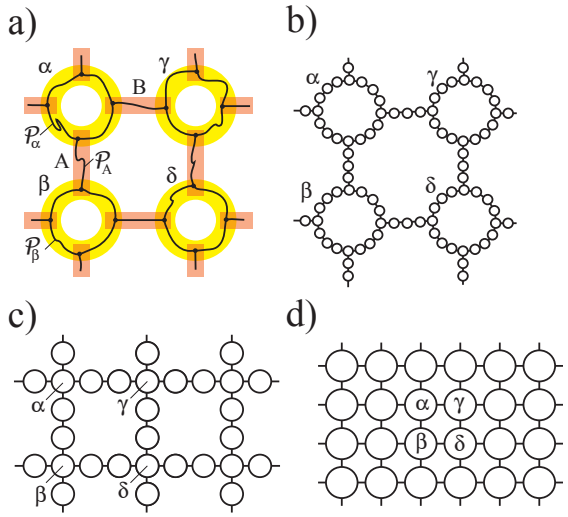

FIG. 4: Transforming $|G(\mathcal{A}\rangle$ into a 2D cluster state. (a) Macroscopic view: Regions α, β, A etc imposed on the graph $G(\mathcal{A})$. (b) (Part of) the graph G_N. (c) Decorated 2D grid. (d) 2D grid for the cluster state.

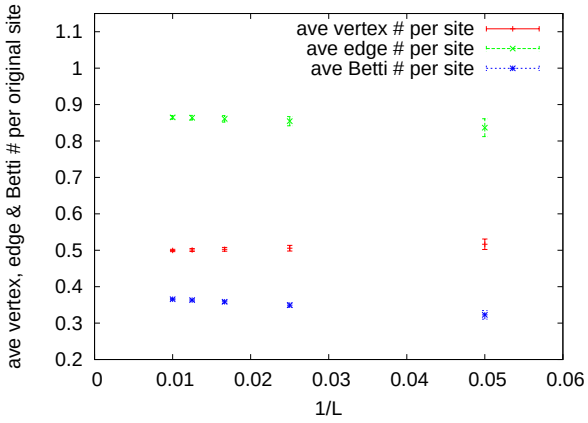

FIG. 5: (color online) Average vertex (or domain) number, average edge number, and average Betti number in the typical random graphs original lattice site vs. L. This shows the number of domains, the number of interdomain Ising interaction, and the number of independent loops in the resultant graph all scale with the system size of the original honeycomb lattice.

angular shape and connect the ring-like regions. If Condition 2 holds then, with probability approaching unity in the limit of large-size α, there exists a loop-like path $\mathcal{P}_\alpha \subset \alpha$. An analogous path exists in the regions β, γ, etc. Furthermore, if Condition 2 holds then in the region A (which is overlapping with both α and β) exists a path $\mathcal{P}_A$ stretching from $\mathcal{P}_\alpha \cap A$ to $\mathcal{P}_\beta \cap A$. Analogous paths exist in the regions B, C, and so on. Wlog, all paths can be taken free of self-intersections. The resulting net G_N of paths is displayed in Fig. 4b.

Now note that the graph state $|G_N\rangle$ can be obtained from $|G(\mathcal{A})\rangle$ by local Z-measurements on all qubits in $G(\mathcal{A})\backslash G_N$. In the present scenario, the graph states $|G_N\rangle$ and $|G(\mathcal{A})\rangle$ are encoded, and the encoded observable $\overline{Z}$ [see Eq. (9)] needs to be measured. Now, using the rules [27] for manipulation of graph states by local measurements

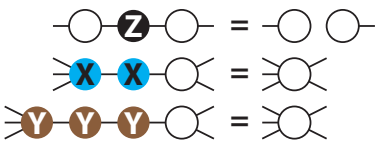

, (A1)

the loops in the graph G_N are contracted into single vertices, and G_N is thereby transformed into the decorated two-dimensional grid displayed in Fig. 4c. Then, again by using the local measurements according to the graph rules Eq. (A1), the decorations in the 2D grid are removed and the standard two-dimensional cluster state is obtained; see Fig. 4d. The 2D cluster state is known to be a universal resource for measurement-based quantum computation [2]. □

Appendix B: Monte Carlo simulations

We give the recipe for performing Monte Carlo simulations and present some results.
(1) First, we randomly assign every site on the honeycomb lattice to be either x, y or z-type with equal probability.
(2) Second, we use the Metropolis method to sample typical configurations. For each site we attempt to flip the type to one of the other two with equal probability. Accept the flip with a probability $p_{\text{accept}} = \min\left\{1, 2^{|V'|-|E'|-|V|+|E|}\right\}$, where $|V|$ and $|E|$ denote the number of domains and inter domain edges (before the contraction steps (2a) and (2b) in Sec. III), respectively before the flip, and similarly $|V'|$ and $|E'|$ for the flipped configuration. The counting of $|V|$ and $|E|$, etc. is done via a generalized Hoshen-Kopelman algorithm [25]. For the proof of the probability ratio, see Appendix C.

(3) After many flipping events, we measure the properties regarding the graph structure for the domains and study their percolation properties upon deleting edges. For the percolation, we cut open the lattice and investigate the percolation threshold for the typical random graphs from the Metropolis sampling.

Figure 2 shows the average degree of a vertex vs. inverse system length $1/L$ for the random graphs, as well as the average numbers of the original sites contained in a typical domain and the width in the domain size distribu-

tion. It extrapolates to $\bar{d} \approx 3.52$ for the infinite system. In Fig. 5 we show the size dependence of average vertex number, average edge number, and average Betti number B [26] of the graph for the graph state per original lattice site for the graph formed by the domains. We have $|\bar{V}| \approx 0.496L^2$, $|\bar{E}| \approx 0.872L^2$, and $\bar{B} \approx 0.377L^2$. This shows that the typical random graph of the graph state retains large number of vertices, edges, and cycles, giving strong evidence that the state is a universal resource. In order to show the stability of the random graph, we investigate how robust it is upon, e.g., deleting edges probabilistically, i.e., the bond percolation. As shown in Fig. 3, it requires the probability of deleting to be as high $p_{\rm delete} \approx 0.43$ (i.e., percolation threshold $p_{\rm th} \approx 0.57$) in order to destroy the spanning property of the graph. Percolation argument was previously employed by Kieling, Rudolph, and Eisert in establishing the universality of using nondeterministic gates to construct a universal cluster state [28].

Appendix C: Evaluation of probability ratio

For convenience, we shall use spin-3/2 representation of the AKLT state. The location projection operator is hence

$$\hat{P}_v = |1\rangle\langle 000| + |2\rangle\langle 111| + |3\rangle\langle W| + |4\rangle\langle \overline{W}| \qquad \text{(C1)}$$

where we have simplified the notation for the spin-3/2 basis states: $|1\rangle \equiv |3/2, 3/2\rangle$, $|2\rangle \equiv |3/2, -3/2\rangle$, $|3\rangle \equiv |3/2, 1/2\rangle$ and $|4\rangle \equiv |3/2, -1/2\rangle$. The AKLT state can then be expressed as

$$|\psi\rangle_{\rm AKLT} = \bigotimes_v \hat{P}_v \prod_{e=(u,v)\in E} |\phi\rangle_e, \qquad \text{(C2)}$$

where $|\phi\rangle_e$ is the singlet state $(|01\rangle - |10\rangle)_{u_i,v_j}$ for the edge $e = (u, v)$ and i, j specify the virtual qubit in the respective vertex.

The POVM that reduces the spin-3/2 AKLT to a spin-1/2 graph state consists of elements $E_\mu = F_\mu^\dagger F_\mu$ such that $\mathbb{1} = E_x + E_y + E_z$, with

$$\hat{F}_z = \hat{F}_z^\dagger \equiv \sqrt{\frac{2}{3}}(|1\rangle\langle 1| + |2\rangle\langle 2|) = \frac{1}{\sqrt{6}}\big(S_z^2 - \frac{1}{4}\big), \quad \text{(C3)}$$

$$\hat{F}_x = \hat{F}_x^\dagger \equiv \sqrt{\frac{2}{3}}(|a\rangle\langle a| + |b\rangle\langle b|) = \frac{1}{\sqrt{6}}\big(S_x^2 - \frac{1}{4}\big), \quad \text{(C4)}$$

$$\hat{F}_y = \hat{F}_y^\dagger \equiv \sqrt{\frac{2}{3}}(|\alpha\rangle\langle \alpha| + |\beta\rangle\langle \beta|) = \frac{1}{\sqrt{6}}\big(S_y^2 - \frac{1}{4}\big), \quad \text{(C5)}$$

where we have also expressed $\hat{F}$'s in terms of the corresponding spin operators. The other four states other than $|1\rangle$ and $|2\rangle$ are

$$|a\rangle \equiv \frac{1}{\sqrt{8}}(|1\rangle + |2\rangle + \sqrt{3}|3\rangle + \sqrt{3}|4\rangle) \qquad \text{(C6)}$$

$$|b\rangle \equiv \frac{1}{\sqrt{8}}(|1\rangle - |2\rangle - \sqrt{3}|3\rangle + \sqrt{3}|4\rangle) \qquad \text{(C7)}$$

$$|\alpha\rangle \equiv \frac{1}{\sqrt{8}}(|1\rangle - i|2\rangle + i\sqrt{3}|3\rangle - \sqrt{3}|4\rangle) \qquad \text{(C8)}$$

$$|\beta\rangle \equiv \frac{1}{\sqrt{8}}(|1\rangle + i|2\rangle - i\sqrt{3}|3\rangle - \sqrt{3}|4\rangle). \qquad \text{(C9)}$$

They correspond to the four virtual three-spin-1/2 states (in addition to $|000\rangle$ and $|111\rangle$) $|++{+}\rangle, |--{-}\rangle| \; i \; i \; i\rangle$ and $|{-}i, {-}i, {-}i\rangle$.

While the outcome of POVM constructed above at each site is random (either x, y or z), outcomes at different sites may be correlated. For a particular set of outcomes $\{a_v\}$ at sites $\{v\}$, the resultant state is transformed to the following un-normalized state

$$|\psi'\rangle = \bigotimes_v \hat{F}_{v,a_v}|\psi\rangle_{\rm AKLT}, \qquad \text{(C10)}$$

with the probability being

$$p_{\{a_v\}} = \langle\psi'|\psi'\rangle / \langle\psi|\psi\rangle_{\rm AKLT}. \qquad \text{(C11)}$$

As $\hat{F}$'s are proportional to projectors, in evaluating the relative probability for two sets of outcome $\{a_v\}$ and $\{b_v\}$, one has

$$p_{\{a_v\}}/p_{\{b_v\}} = \langle\psi|\bigotimes_v \hat{F}_{v,a_v}|\psi\rangle_{\rm AKLT} / \langle\psi|\bigotimes_v \hat{F}_{v,b_v}|\psi\rangle_{\rm AKLT}. \qquad \text{(C12)}$$

In order to evaluate the probability ratio for two different sets of configuration, we first note that

$$\hat{F}_x\hat{P} \sim |a\rangle\langle +++| + |b\rangle\langle ---| \qquad \text{(C13)}$$

$$\hat{F}_y\hat{P} \sim |\alpha\rangle\langle i\,i\,i| + |\beta\rangle\langle -i\,-i\,-i| \qquad \text{(C14)}$$

$$\hat{F}_z\hat{P} \sim |1\rangle\langle 000| + |2\rangle\langle 111|. \qquad \text{(C15)}$$

The spin-3/2 state is transformed by $\bigotimes_v F_{v,a_v}$ to an effective spin-1/2 one, with the two levels being labeled by (a, b), (α, β), or $(1, 2)$, depending on which $\hat{F}$ is applied. The probability $p_{\{a_v\}}$ is essentially obtained by summing the square norm of the coefficients for all possible spin-1/2 constituent basis states (e.g. $|a\,b + 0\,i\ldots\rangle$ is a basis state). First we need to know how many different constituent states, and the number is related to how many effective spin-1/2 particles we have. For the sites that have same type of outcome (x, y or z), they basically form a superposition of two Neél-like states, thereby corresponding to an effective spin-1/2 particle. This can be seen from the valence-bond picture that, e.g., for $r, s \in \{0, 1\}$ we have $\langle rs|01 - 10\rangle = \pm\delta_{r,1-s}$. On the other hand, for $r \in \{0, 1\}$ and $s \in \{+, -\}$, $\langle rs|01 - 10\rangle = \pm 1/\sqrt{2}$, which is $1/\sqrt{2}$ smaller than if r and s are the indices

in the same basis. This means that all four combinations $\{0+, 0-, 1+, 1-\}$ occur with equal amplitude up to a phase. (Similar consideration applies to other combinations of bases.) Therefore, the number of effective spin-1/2 particles is given by the number of domains, which we label by $|V|$. Notice that we have assumed that any domain does not contain a cycle with odd number of original sites, as no Neél state can be supported on such a cycle (or loop). Fortunately, the honeycomb lattice is bi-partite and therefore any cycle must contain even number of sites.

What about the amplitude for each spin configuration? Furthermore, what is the probability of obtaining a particular set of outcome $\{a_v\}$? We have seen that for each inter-domain edge there is a contribution to a factor of $1/\sqrt{2}$ in the amplitude (as the end sites of the edge correspond to different types). Thus, the amplitude for each spin configuration gives an overall value (omitting the phase factor) of $2^{-|E|/2}$ and hence an probability weight $2^{-|E|}$, where $|E|$ counts the number of inter-domain edges. As there are $2^{|V|}$ such configurations, we have the norm square of the resultant spin-1/2 state being proportional to $p \sim 2^{|V|-|E|}$. For convenience, we have assume the lattice is periodic. Moreover, for all sites having the same type, we count $|E| = 0$ and $|V| = 1$.

Appendix D: Reducing 1D AKLT state to a 1D cluster state

Chen et al. [19] have recently shown that the 1D AKLT state can be locally reduced to a 1D cluster state with a random length. We show that a similar POVM to our 2D case can also be used to give an alternative proof of the reduction. Recall that the 1D AKLT state can be obtained by making local projection on a underlying singlet valence bond structure:

$$\hat{P}_i = |1\rangle\langle 00| + |-1\rangle\langle 11| + |0\rangle\langle\psi^+|, \quad \text{(D1)}$$

$$|\psi^+\rangle \equiv \frac{1}{\sqrt{2}}(|01\rangle + |10\rangle). \quad \text{(D2)}$$

To simplify the analysis, let us assume even number of lattice sites and periodic boundary condition. The POVM, $\mathbb{1} = E_x + E_y + E_z$ with $E_\mu = F_\mu^\dagger F_\mu$, is similar to the spin-3/2 case,

$$F_z \equiv \sqrt{\frac{1}{2}}(|1\rangle\langle 1| + |-1\rangle\langle -1|) = \sqrt{\frac{1}{2}}\, S_z^2, \quad \text{(D3)}$$

$$F_x \equiv \sqrt{\frac{1}{2}}(|a\rangle\langle a| + |b\rangle\langle b|) = \sqrt{\frac{1}{2}}\, S_x^2, \quad \text{(D4)}$$

$$F_y \equiv \sqrt{\frac{1}{2}}(|\alpha\rangle\langle\alpha| + |\beta\rangle\langle\beta|) = \sqrt{\frac{1}{2}}\, S_y^2, \quad \text{(D5)}$$

where the other four states other than $|1\rangle$ and $|-1\rangle$ are

$$|a\rangle \equiv \frac{1}{2}(|1\rangle + |-1\rangle + \sqrt{2}|0\rangle) \quad \text{(D6)}$$

$$|b\rangle \equiv \frac{1}{2}(|1\rangle + |-1\rangle - \sqrt{2}|0\rangle) \quad \text{(D7)}$$

$$|\alpha\rangle \equiv \frac{1}{2}(|1\rangle - |-1\rangle + i\sqrt{2}|0\rangle) \quad \text{(D8)}$$

$$|\beta\rangle \equiv \frac{1}{2}(|1\rangle - |-1\rangle - i\sqrt{2}|0\rangle). \quad \text{(D9)}$$

They correspond to the four virtual three-spin-1/2 states (in addition to $|00\rangle$ and $|11\rangle$) $|++\rangle$, $|--\rangle$, $|\,i\,i\rangle$ and $|-i, -i\rangle$. After the POVM is performed at all sites, each physical site will become an effective spin-1/2 particle.

The proof of the encoded graph state in the honeycomb lattice carries over to one-dimensional chain here, and so does the reduction of a domain to a single site by using appropriate local measurement (except we need to pay attention to a cycle with odd number of sites). The probability of a particular set of POVM outcome of (x, y, z) is thus proportional to $P \sim 2^{|V|-|E|}$, carried over from the 2D case, unless all local POVM outcomes are the same, which has $P \sim 2$ (note that this cannot occur in the case of odd number chain) with all other cases having $P \sim 1$, as $|V| = |E|$ for a 1D cycle. The typical graph will have a length roughly a constant fraction of the original size, which is consistent with the results obtained in Ref. [19]. The average length of the resultant 1D cluster in the large-system limit is 2/3 of the original AKLT chain size. Hence, it can be used to implement an arbitrary one-qubit unitary gate. This gives an alternative proof of the results in Ref. [19] for the reduction of 1D AKLT state to a 1D cluster state.

Appendix E: Calculation of probability of a particular POVM outcome using AHH techniques

In this appendix we provide an alternative formulation to the calculation of POVM outcome probability. This formalism has the potential of being applicable to a more general case. We give only the important ingredients here.

Arovas, Auerbach and Haldane (AAH) [20] show how to represent arbitrary AKLT states as Boltzmann weights for nearest neighbour statistical mechanical models in the same spatial dimension as the quantum problem and how to represent calculations of equal time ground state expectation values classically. We are interested in two cases: the $S = 1$ one-dimensional case and the $S = 3/2$ honeycomb lattice case.

In both cases the operators of interest are projection operators onto maximal $|S^z|$:

$$F_\nu \equiv (S_\nu)^2, \quad (S = 1) \quad \text{(E1)}$$

$$\equiv (1/2)[(S_\nu)^2 - 1/4], \quad (S = 3/2), \quad \text{(E2)}$$

where $\nu = x, y$ or z and, for convenience, we have rescaled the prefactor in the definition of F's. For general spin

S the operators S_μ are represented first in terms of Schwinger bosons, a, $a^\dagger$, b, $b^\dagger$, then in terms of coordinates and derivatives u, v, ∂_u, ∂_v then in terms of u, v, u^*, v^*. The operator $(S_z)^2$ is:

$$(S_z)^2 = (1/4)(a^\dagger a - b^\dagger b)^2 = (1/4)a^2(a^\dagger)^2 + (1/4)b^2(b^\dagger)^2 - (1/4)(a^\dagger a + b^\dagger b + 2) \quad \text{(E3)}$$

$$= (1/4)[\partial_u^2 u^2 + \partial_v^2 v^2 - 2S - 2] \to (1/4)(2S+2)(2S+3)(|u|^2 - |v|^2)^2 - (1/2)(S+1). \quad \text{(E4)}$$

Using $u = \cos(\theta/2)e^{i\phi/2}$, $v = \sin(\theta/2)e^{-i\phi/2}$, where θ and ϕ are the polar and azimuthal angles on the unit sphere, this becomes:

$$(S^z)^2 = (1/4)(2S+2)(2S+3)(\Omega^z)^2 - (1/2)(S+1) \quad \text{(E5)}$$

where $\hat{\Omega} = (\cos\theta\cos\phi, \sin\theta\sin\phi, \cos\theta)$ is the unit vector.

A simple explicit calculation similar to this one shows that, for $\nu = x$, y or z:

$$(S_\nu)^2 = (1/4)(2S+2)(2S+3)(\Omega^\nu)^2 - (1/2)(S+1) \quad \text{(E6)}$$

as expected by SO(3) symmetry. This is a somewhat surprising formula in that the classical quantities are not positive semi-definite. Note that this formula is valid independent of the wave-function. The projection operators thus become:

$$F_\nu = 5(\Omega^\nu)^2 - 1, \quad (S=1) \quad \text{(E7)}$$

$$= (3/4)[5(\Omega^\nu)^2 - 1], \quad (S = 3/2). \quad \text{(E8)}$$

Remarkably the projection operators are the same for $S = 1$ and $3/2$ up to an unimportant normalization factor.

The AKLT state can be written, in Schwinger boson notation as:

$$|\psi\rangle_{\rm AKLT} = \prod_{<i,j>} (a_i^\dagger b_j^\dagger - a_j^\dagger b_i^\dagger)|\text{vacuum}\rangle \to \prod_{<i,j>} [1 - \hat{\Omega}_i \cdot \hat{\Omega}_j]. \quad \text{(E9)}$$

where the product is over all pairs of neighbouring sites (i, j) . Actually, we need to be more precise about boundary conditions here. These details will be discussed elsewhere. Using the form of the AKLT state we wish to calculate:

$$p_{a_1 a_2 \ldots a_N} \equiv \mathcal{N}_S \frac{1}{Z} \prod_{i=1}^{N} \int d\hat{\Omega}_i [5(\Omega_i^{a_i})^2 - 1] \prod_{<j,k>} [1 - \hat{\Omega}_j \cdot \hat{\Omega}_j] \quad \text{(E10)}$$

where Z is the same integral without the $[5(\Omega_i^{a_i})^2 - 1]$ factors and $\mathcal{N}_S = 1$ for $S = 1$ and $(3/4)^N$ for $S = 3/2$. In both cases we can evaluate this by multiplying out $\prod_{<j,k>}[1 - \hat{\Omega}_j \cdot \hat{\Omega}_k]$.

We remark that carrying out this we arrive at the same conclusion of the probability expressions for 1D chain and 2D honeycomb cases as before.

[1] M. Nielsen and I. Chuang, *Quantum Computation and Quantum Information* (Cambridge Univ. Press, 2000).

[2] R. Raussendorf and H. J. Briegel, Phys. Rev. Lett. **86**, 5188 (2001); R. Raussendorf, D. E. Browne and H. J. Briegel, Phys. Rev. A **68**, 022312 (2003); H. J. Briegel, D. E. Browne, W. Dür, R. Raussendorf, and M. Van den Nest, Nature Physics **5**, 19 (2009).

[3] H. J. Briegel and R. Raussendorf, Phys. Rev. Lett. **86**, 910 (2001).

[4] R. Prevedel, P. Walther, F. Tiefenbacher, P. Böhi, R. Kaltenbaek, T. Jennewein, and A. Zeilinger, Nature **445**, 65 (2006). C.-Y. Lu, X.-Q. Zhou, O. Guehne, W.-B. Gao, J. Zhang, Z.-S. Yuan, A. Goebel, T. Yang, and J.-W. Pan, Nat. Phys. **3**, 91 (2007). H. S. Park, J. Cho, J. Y. Lee, D.-H. Lee, and S.-K. Choi, Opt. Express **15**, 17960 (2007).

[5] O. Mandel, M. Greiner, A. Widera, T. Rom, T. W. Hänsch, and I. Bloch, Nature (London) **425**, 937 (2003).

[6] M. A. Nielsen, e-print arXiv:quant-ph/0504097.

[7] S. D. Bartlett and T. Rudolph, Phys. Rev. A, **74**, 040302(R) (2006).

[8] F. Verstraete and J. I. Cirac, Phys. Rev. A **70** 060302(R) (2004).

[9] D. Gross and J. Eisert, Phys. Rev. Lett. **98**, 220503 (2007); D. Gross, J. Eisert, N. Schuch, and D. Perez-Garcia, Phys. Rev. A **76**, 052315 (2007); D. Gross and J. Eisert, e-print arXiv:0810.2542.

[10] I. Affleck, T. Kennedy, E. H. Lieb, and H. Tasaki, Phys. Rev. Lett. **59**, 799 (1987); Comm. Math. Phys. **115**, 477 (1988). T. Kennedy, E. H. Lieb, and H. Tasaki, J. Stat. Phys. **53**, 383 (1988).

[11] F. D. M. Haldane, Phys. Lett. A **93**, 464 (1983); Phys.

Rev. Lett. **50**, 1153 (1983).
[12] A. Miyake, Phys. Rev. Lett. **105**, 040501 (2010).
[13] J. Lavoie, R. Kaltenbaek, B. Zeng, S. D. Bartlett, and K. J. Resch, to appear in Nature Physics.
[14] G. K. Brennen and A. Miyake, Phys. Rev. Lett. **101**, 010502 (2008).
[15] X. Chen, B. Zeng, Z.-C. Gu, B. Yoshida, and I. L. Chuang, Phys. Rev. Lett. **102**, 220501 (2009).
[16] J.-M. Cai, A. Miyake, W. Dür, and H. J. Briegel, arXiv:1004.19071v1
[17] M. Van den Nest, A. Miyake, W. Dür, and H. J. Briegel, Phys. Rev. Lett. **97**, 150504 (2006).
[18] J.-M. Cai, W. Dür, M. Van den Nest, A. Miyake, and H. J. Briegel, Phys. Rev. Lett. **103**, 050503 (2009).
[19] X. Chen, R. Duan, Z. Ji, and B. Zeng, Phys. Rev. Lett. **105**, 020502 (2010).
[20] D. Arovas, A. Auerbach and F.D.M. Haldane, Phys. Rev. Lett. **60**, 531 (1988).
[21] D. Gottesman, *Stabilizer Codes and Quantum Error Correction*, Ph.D. Thesis, Caltech (1997); also in e-print arXiv:quant-ph/9705052.
[22] An adjacency matrix $A(\mathcal{G})$ of graph $\mathcal{G}$ describes the structure of the graph: $[A(\mathcal{G})]_{uv} = 1$ if (u, v) is an edge, and zero otherwise.
[23] The three elements F's can also be rewritten as

$$\begin{aligned} F_{v,z} &= \sqrt{\frac{2}{3}}(|000\rangle\langle 000| + |111\rangle\langle 111|) \\ F_{v,x} &= \sqrt{\frac{2}{3}}(|+++\rangle\langle +++| + |---\rangle\langle ---|) \\ F_{v,y} &= \sqrt{\frac{2}{3}}(|i,i,i\rangle\langle i,i,i| + |-i,-i,-i\rangle\langle -i,-i,-i|), \end{aligned}$$

where $|\pm\rangle \equiv (|0\rangle \pm |1\rangle)/\sqrt{2}$ and $|\pm i\rangle \equiv (|0\rangle \pm i|1\rangle)/\sqrt{2}$. From this, it is apparent that the three operators are rank-two and the structure of the effective two levels is also explicit.
[24] D.E. Browne et al., New J. Phys. **10**, 023010 (2008).
[25] J. Hoshen and R. Kopelman, Phys. Rev. B **14**, 3438 (1976).
[26] The Betti number of a graph G is defined as $B \equiv |E(G)| - |V(G)| + 1$, and it counts the number of independent cylcles.
[27] M. Hein, J. Eisert, and H.-J. Briegel, Phys. Rev. A **69**, 062311 (2004); M. Hein, W. Dr, J. Eisert, R. Raussendorf, M. Van den Nest, and H.-J. Briegel, e-print arXiv:quant-ph/0602096v1.
[28] K. Kieling, T. Rudolph, and J. Eisert, Phys. Rev. Lett. **99**, 130501 (2007).